# USING COLORS TO IMPROVE PHOTOMETRIC METALLICITY ESTIMATES FOR GALAXIES

N. E. Sanders[1], E. M. Levesque[2,3], A. M. Soderberg[1]
*Draft version June 22, 2021*

## ABSTRACT

There is a well known correlation between the mass and metallicity of star-forming galaxies. Because mass is correlated with luminosity, this relation is often exploited, when spectroscopy is not available, to estimate galaxy metallicities based on single band photometry. However, we show that galaxy color is typically more effective than luminosity as a predictor of metallicity. This is a consequence of the correlation between color and the galaxy mass-to-light ratio and the recently discovered correlation between star formation rate (SFR) and residuals from the mass-metallicity relation. Using Sloan Digital Sky Survey spectroscopy of $\sim 180,000$ nearby galaxies, we derive "$LZC$ relations," empirical relations between metallicity (in seven common strong line diagnostics), luminosity, and color (in ten filter pairs and four methods of photometry). We show that these relations allow photometric metallicity estimates, based on luminosity and a single optical color, that are $\sim 50\%$ more precise than those made based on luminosity alone; galaxy metallicity can be estimated to within $\sim 0.05 - 0.1$ dex of the spectroscopically-derived value depending on the diagnostic used. Including color information in photometric metallicity estimates also reduces systematic biases for populations skewed toward high or low SFR environments, as we illustrate using the host galaxy of the supernova SN 2010ay. This new tool will lend more statistical power to studies of galaxy populations, such as supernova and gamma-ray burst host environments, in ongoing and future wide field imaging surveys.

*Subject headings:* galaxies: abundances — galaxies: photometry — galaxies: ISM

## 1. INTRODUCTION

The gas-phase metallicity of galaxies, as measured from their nebular emission spectrum, is correlated with galaxy luminosity (Lequeux et al. 1979; Garnett & Shields 1987). This relation has been used as a key observational tool in the study of populations such as supernova host galaxies (e.g. Prantzos & Boissier 2003; Arcavi et al. 2010), where gas-phase metallicity is an important proxy for the properties of their short lived progenitor stars. However, using Sloan Digital Sky Survey (SDSS) imaging and spectroscopy for $\sim 53,000$ galaxies, Tremonti et al. (2004) showed that the luminosity-metallicity relation has a large intrinsic scatter of $\sigma = 0.16$ dex (50%), in terms of metallicity residuals, which limits the utility of this relation as an effective indicator of metallicity.

There are two primary causes for the scatter in the luminosity-metallicity relation. First, while the scatter in the *mass*-metallicity relation is fairly small ($\sigma = 0.10$ dex, Tremonti et al. 2004), luminosity is not a perfect proxy for mass. The mass-to-light ratio of galaxies is highly correlated with galaxy color, such that redder galaxies at a fixed luminosity are more massive (Bell & de Jong 2001; Kauffmann et al. 2003b). Second, a more fundamental relation has been uncovered between mass (M), metallicity ($Z$), and star formation rate (SFR) (Lara-López et al. 2010; Mannucci et al. 2010). This "fundamental plane" or "Fundamental Metallicity Relation" has remarkably small residual scatter ($\sigma = 0.05$ dex), in-

dicating that variations in SFR are responsible for much of the scatter in the mass-metallicity relation. The existence of this fundamental plane is a valuable constraint for models of galaxy evolution, and likely an expression of galaxy outflows, infall, downsizing, and/or gas-rich mergers (Mannucci et al. 2010; Peeples & Shankar 2011; Yates et al. 2012). To improve the precision of photometric metallicity estimates, a readily accessible observable must be used to break the degeneracy between luminosity, mass, and SFR.

In this paper, we show that the addition of color information significantly decreases the scatter in photometric metallicity estimates. We derive the optimal projection of the fundamental plane for star-forming galaxies, in terms of the observable properties luminosity and color, that we call the $LZC$ relation. We describe the sample of SDSS galaxies we use to study these correlations and methods for spectroscopic metallicity estimation in Section 2. In Section 3, we derive analytic expressions for the $LZC$ as expressed in a variety of different filter sets, methods of photometry, and metallicity diagnostics and we discuss the limitations of these calibrations in Section 4. Finally, in Section 5, we describe how specific observational studies may benefit from the $LZC$ relation in making precise metallicity determinations from imaging available from wide field sky surveys.

## 2. GALAXY SAMPLE

We used spectroscopic data and derived quantities from the MPA/JHU catalog[4] of $927,552$ star-forming galaxies from the SDSS-DR7 (Abazajian et al. 2009).[5]

nsanders@cfa.harvard.edu
[1] Harvard-Smithsonian Center for Astrophysics, 60 Garden Street, Cambridge, MA 02138 USA
[2] CASA, Department of Astrophysical and Planetary Sciences, University of Colorado, 389-UCB, Boulder, CO 80309, USA
[3] Einstein Fellow

[4] The MPA/JHU catalog is available at http://www.mpa-garching.mpg.de/SDSS
[5] We assume a standard ΛCDM cosmology throughout this work, adopting the Hubble constant $H_0 = 73$ km s$^{-1}$ Mpc$^{-1}$, $\Omega_m = 0.3$,

The catalog includes emission line fluxes, stellar masses (based on SED fitting to $ugriz$ photometry), and star formation rates for each galaxy, as described in Kauffmann et al. (2003b); Brinchmann et al. (2004); Salim et al. (2007). While the MPA/JHU line fluxes are corrected for Galactic extinction, we additionally correct them for intrinsic reddening using the Balmer flux decrement. The fluxes are measured on continuum-subtracted spectra and therefore the H$\alpha$ and H$\beta$ line fluxes are corrected for Balmer absorption from the underlying stellar population (Tremonti et al. 2004). We assume $F_{H\alpha}/F_{H\beta} = 2.85$ (corresponding to $T = 10,000$ K and $n_e = 10^4$ cm$^{-3}$ for Case B recombination; Osterbrock & Ferland 2006) and the extinction curve of Cardelli et al. (1989), assuming $R_V = 3.1$.

We joined the MPA/JHU catalog data with the photometric data from the SDSS-DR9 (Ahn et al. 2012). To compare the effects of different methods of photometry, we include the SDSS model, cModel, Petrosian, and 3″ fiber magnitudes (for details see Stoughton et al. 2002). We adopt the model/cModel and Petrosian magnitude $K$-corrections provided in the NYU Value Added Galaxy Catalog (Blanton et al. 2005; Blanton & Roweis 2007; Padmanabhan et al. 2008), and for the fiber magnitudes we adopt the $K$-corrections from the MPA/JHU catalog (only available for the $g, r, i$ filters).[6] We correct the photometry for foreground Galactic dust extinction (Schlegel et al. 1998).

We perform preliminary sample cuts on the catalog following a modified version of the prescription of Mannucci et al. (2010), as follows. First, we require that the galaxy be included in the SDSS MAIN spectroscopic sample, i.e. $r < 17.77$ mag after Galactic redenning correction. Second, we limit the sample to galaxies with $0.03 < z < 0.3$. This guarantees the availability of [O II] $\lambda3727$ and is more inclusive than the $0.07 < z < 0.3$ cut of Mannucci et al. 2010. Third, we adopt the data quality cut from Mannucci et al. (2010), $(S/N)_{H_\alpha} > 25$, $F_{H\alpha}/F_{H\beta} > 2.5$, which they chose to provide high data quality (high signal to noise and not saturated) in all relevant emission lines without biasing the sample explicity towards higher metallicities. Fourth, we require the fraction of the $r$-band flux within the SDSS fiber to the full Petrosian flux to be $> 0.05$, to exclude $\sim 0.1\%$ galaxies where the SDSS spectroscopy includes very little of the total flux and may not reflect the galaxy global properties.

Fifth, we reject AGN following Kauffmann et al. (2003a). Finally, we require that $K$ corrections be available (see methodology below) and that the derived metallicitiy (see methodology below) be within a reasonable physical range ($7 < \log(O/H) + 12 < 9.5$). We make no selection based on the internal extinction within the galaxies ($A_V$; Mannucci et al. 2010 excluded high-reddening galaxies).

For each galaxy, we compute oxygen abundance as a proxy for metallicity using a variety of strong line diagnostics that are widely used in the literature (Table 1; see Lopez-Sanchez et al. 2012 for a recent review). First, we employ several diagnostics relying on the R23 ratio, which depends on the fluxes of O II $\lambda\lambda 3726, 3729$, O III $\lambda 4959$ and $\lambda 5007$, and H$\beta$. The R23 diagnos-

and $\Lambda = 0.7$.

[6] All $K$-corrections are made to the $z = 0$ frame.

TABLE 1
METALLICITY DIAGNOSTICS USED

| Name | Method | Source |
|------|--------|--------|
| M91 | R23 | McGaugh 1991[a] |
| KD02 | N2O2 | Kewley & Dopita 2002[b] |
| KK04 | R23 | Kobulnicky & Kewley 2004 |
| PP04 | N2,O3N2 | Pettini & Pagel 2004 |
| T04 | model[c] | Tremonti et al. 2004 |
| PVT | $P$ | Pilyugin et al. 2010[d] |

[a] We have adopted the revised prescription suggested by Kobulnicky et al. (1999).
[b] Following Kewley & Ellison (2008), we adopt the average of the M91 and KK04 for the lower branch solution.
[c] The T04 metallicities are estimated based on simultaneous fits of all major emission lines to photoionization models and are provided in the MPA/JHU catalog
[d] We use the "ONS" solution, which includes a dependence on the S II flux, for the conditions $\log(N2) > -0.1$ and $\log(N2/S2) > -0.25$ (which is true for $\sim 98\%$ of the SDSS galaxies).

tic suffers from a degeneracy (see e.g. Kewley & Dopita 2002) that we break using either the N2O2 (N II $\lambda6584$ to O II $\lambda3727$) or N2 (N II $\lambda6584$ to H$\alpha$) ratios, following the authors' prescriptions. Next we employ diagnostics depending on N2, N2O2, and O3N2, the flux ratio of O III $\lambda5007$ and N II $\lambda6584$. Finally, we employ diagnostics based on the ionization parameter, $P$, the ratio of O III $\lambda4959$ and $\lambda5007$ to R23. It is necessary to calibrate for multiple diagnostics because they exhibit well known systematic discrepancies, which are particularly strong between those diagnostics calibrated empirically and those calibrated against photoionization models (Kewley & Ellison 2008). Yates et al. (2012) have already shown that the fundamental metallicity relation varies with the diagnostic used.

The number of galaxies in our final sample, following the cuts described, varies somewhat with the choice of filter set, photometric system, and metallicity diagnostic. We consider $\sim (110 - 120) \times 10^3$ galaxies with T04 metallicities and $\sim (160 - 180) \times 10^3$ galaxies for other metallicity diagnostics.

Figure 1 demonstrates two correlations in the galaxy sample. First, it shows the well known luminosity-metallicity correlation (shown using $M_g$), where more luminous galaxies typically have higher metallicities. However, there is significant scatter in this relation, with a standard deviation of $\sigma_0 = 0.13$ dex in the metallicity residuals from the $g$ band luminosity-metallicity relation. Second, the figure demonstrates that there is a correlation between the residual in metallicity (the offset from the luminosity-metallicity relation) and galaxy color.

### 3. LUMINOSITY-METALLICITY-COLOR RELATION

Following Mannucci et al. (2010), we project the $LZC$ relation onto an axis $\mu$ with components of color and luminosity:

$$\mu = M_i - \alpha \times (m_i - m_j) \quad (1)$$

$$12 + \log(O/H) = p_0 + p_1\,\mu + p_2\,\mu^2 + p_3\,\mu^3 \quad (2)$$

where $i, j$ are choices of filters and $p_l$ are parameters of a third order polynomial. For each combination of metal-
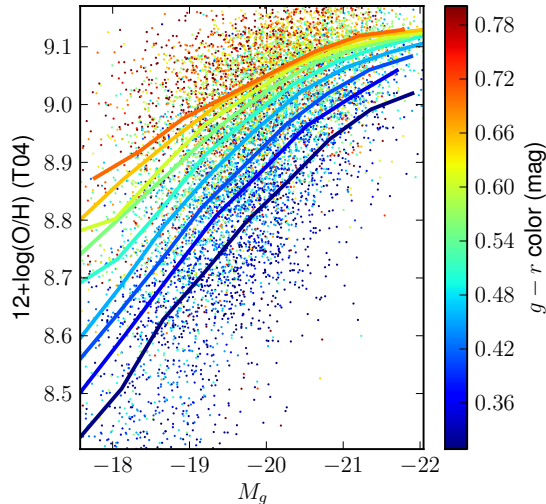
FIG. 1.— A luminosity-metallicity ($g$-band, T04 metallicity, Model magnitudes) plot showing a random subset of $10,000$ SDSS galaxies, color coded by $g - r$ color. The solid lines show the median luminosity-metallicity relation for the galaxies divided into 10 equal-sample-size bins in $g - r$ color.

licity diagnostic, luminosity band, and color, we determine the optimal projection of the galaxy $LZC$ relation by sampling from a grid of $\alpha$ parameters and selecting the value that minimizes the variance in the residuals of metallicity. We calculate the best-fit polynomial using the median value for metallicity in 15 equally-spaced bins along the projected axis, as shown in Figure 2. We report the optimal value of $\alpha$ and corresponding best fit $LZC$ parameters $p$ in Table 2 (for $\alpha$ values in terms of the physical parameters mass and SFR, see Andrews & Martini 2013).

We find a correlation between the luminosity-metallicity relation and color which varies in strength depending on the choice of metallicity diagnostic and filter set. Figure 2 demonstrates this optimization for one filter set $(g, r)$ and three choices of metallicity diagnostic: T04, KD02, and PP04 O3N2. For PP04 O3N2, the scatter in the metallicity residuals of the $LZC$ relation is $\sigma_Z = 0.07$ dex, as compared to the LZ relation ($\alpha = 0$), $\sigma_{Z,0} = 0.10$ dex (an improvement of 37% on a linear scale).

The decrease in residual scatter is similar in other metallicity diagnostics, ranging from $17 - 51\%$. For further statistics, see Table 2.

A nominal correction for the mass-to-light ratio only will account for much, but not all, of the reduction in scatter. For example, for $M_g$ and $(g - r)$, $\alpha = 5.4$ would correspond to the mass-to-light ratio necessary to convert luminosity ($M_g$) to stellar mass (Kauffmann et al. 2003b), but this value of $\alpha$ is smaller than the optimal value in any metallicity diagnostic ($\alpha \sim 6 - 19$, see Table 2).

Note that, regardless of the choice of diagnostic or filters, the residual scatter is lower for asymptotically high values of $\alpha$ than it is for $\alpha = 0$. This implies that, in general, color is more effective than luminosity as a predictor of metallicity.

In contrast, the residual scatter achieved by Mannucci et al. (2010) in terms of the optimal projection

of the physical parameters stellar mass ($M_*$) and SFR, $\mu_{0.32} = \log(M_*) - 0.32 \log(\text{SFR})$, was only 0.05 dex. However, estimation of $\mu_{0.32}$ is based on full $ugriz$ imaging and $R \sim 2000$ optical spectroscopy, while the $LZC$ relation relies on imaging in just two bands and a redshift estimate. The coloring in Figure 2 illustrates that the optimal projection of the photometric properties is highly correlated with $\mu_{0.32}$, with Pearson correlation coefficient $\rho \sim 0.6 - 0.9$ for all metallicity diagnostics and filters. We calculated $\mu_{0.32}$ for the galaxies in our sample using the photometric mass measurement and aperture-corrected SFR estimates from the MPA-JHU catalog.

In general, filter sets that include bluer filters and/or incorporate a greater separation in central wavelengths produce a greater improvement in $\sigma_Z$ (see Figure 3). The three most effective filter combinations are $[g - r, g - i, u - z]$, producing $\sigma_Z/\sigma_{Z,0} = [0.78, 0.80, 0.80]$ (taking the median across all metallicity diagnostics and methods of photometry). The three least effective are $[i - z, u - g, r - i]$, with $\sigma_Z/\sigma_{Z,0} = [0.94, 0.91, 0.91]$.

## 4. CAVEATS

Here we note certain caveats and limitations of the $LZC$ calibrations presented in this work and caution users not to apply them outside of the regime of the calibration data.

First, we recommend that the SDSS model magnitudes be used when applying the $LZC$ relations to estimate galaxy metallicity. Model magnitudes should provide the most accurate measurements of galaxy colors[7], although Petrosian and cModel magnitudes are typically in agreement with model magnitudes to within $< 0.1$ mag. We provide calibrations using the other SDSS photometric methods here for completeness and to support applications to datasets where photometry is only available in a particular method (i.e. Petrosian photometry). Fiber magnitudes, which are integrated over a fixed $3''$ aperture, may not encompass the full galaxy for large or nearby objects. The fiber magnitude calibrations may be useful for explorations of aperture effects (see e.g. Kewley et al. 2005).

Second, the redshift range of the calibration data is $0.03 < z < 0.3$ (Section 2). The $LZC$ relations need to be tested for evolution at higher redshifts due to evolution in the fundamental plane for star-forming galaxies and passive evolution of galaxy colors. It is unclear to what extent the fundamental plane evolution would effect the calibrations. Cresci et al. (2012) found no evolution to $z \sim 0.8$ and Lara-López et al. (2010) concluded that there is no detectable evolution out to $z \sim 3.5$. However, Perez-Montero et al. (2012) investigate a larger sample of $\sim 5000$ zCOSMOS galaxies to $z \sim 1.3$ and report evolution of the SFR-corrected mass-metallicity relation starting at $z \gtrsim 0.4$. As data is assembled to corroborate evolution in these fundamental plane relations, it may also be used to calibrate the redshift dependence of the $LZC$ relations.

Third, redshift estimates are needed to evaluate luminosity and apply $K$-corrections to estimate metallicity using the rest-frame $LZC$ calibrations we present here. Using $ugriz$ photometry of SDSS main sample galaxies ($r < 17.77$ mag, $z < 0.4$), photometric redshift estimates
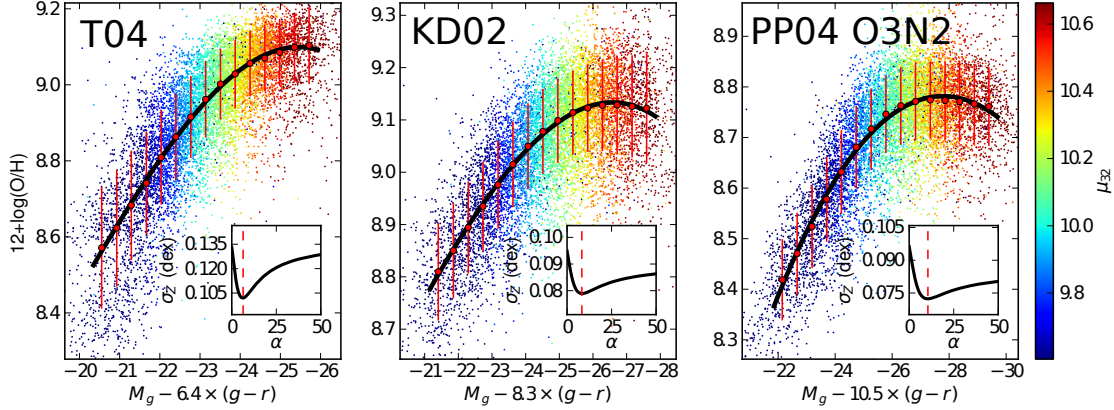
---

[7] http://www.sdss3.org/dr9/algorithms/magnitudes.php)

FIG. 2.— The optimal projection of the $LZC$ relation for $M_g$, $g - r$ color, and three different metallicity diagnostics (T04,KD02, and PP04 O3N2; all in the Model photometric system). The red points and lines show the median and standard deviation of the metallicity for galaxies in 15 bins. The projected $LZC$ relation is shown for the optimal value of $\alpha$, with the best fit third order polynomial $LZC$ relation in black, extending over the calibrated range $(2 - 98\text{th percentile})$. The color coding shows the optical physical parameter $(\mu_{32})$ from Mannucci et al. (2010). The insets display the standard deviation in the residuals in metallicity from the $LZC$ as a function of the color-weighting parameter $\alpha$, with the optimal value marked by the dashed line.

TABLE 2
PARAMETERS OF THE $LZC$ RELATIONS

| $L$ | Color | $\alpha$ | $p_3 \times 10^5$ | $p_2 \times 10^3$ | $p_1 \times 10^3$ | $p_0$ | $\sigma_{Z,0}$ | $\sigma_Z$ | $\sigma_Z/\sigma_{Z,0}$ | $\mu$ range |
|-----|-------|----------|-------------------|-------------------|-------------------|-------|----------------|------------|-------------------------|-------------|
| PP04 O3N2 – model | | | | | | | | | | |
| $u$ | $u - g$ | 5.8 | -98.57 | -94.43 | -2951.55 | -21.48 | 0.100 | 0.087 | 0.867 | [-29.0,-22.8] |
| $u$ | $u - r$ | 4.1 | -55.79 | -59.71 | -2023.09 | -13.30 | 0.100 | 0.079 | 0.784 | [-29.4,-22.7] |
| $u$ | $u - i$ | 3.9 | -83.33 | -82.75 | -2687.82 | -19.90 | 0.100 | 0.078 | 0.778 | [-30.5,-23.5] |
| $u$ | $u - z$ | 3.5 | -47.07 | -51.13 | -1769.68 | -11.02 | 0.100 | 0.076 | 0.762 | [-30.6,-23.0] |
| $g$ | $g - r$ | 10.5 | -9.02 | -18.82 | -836.54 | -1.87 | 0.096 | 0.072 | 0.752 | [-29.7,-21.9] |
| $g$ | $g - i$ | 7.5 | -68.65 | -68.11 | -2210.54 | -14.79 | 0.096 | 0.074 | 0.771 | [-30.5,-23.0] |
| $g$ | $g - z$ | 6.2 | -19.35 | -25.61 | -993.07 | -3.20 | 0.096 | 0.074 | 0.768 | [-30.9,-22.3] |
| $r$ | $r - i$ | 11.0 | -241.03 | -198.54 | -5431.00 | -40.58 | 0.092 | 0.084 | 0.916 | [-26.9,-21.7] |
| $r$ | $r - z$ | 9.6 | -16.28 | -24.51 | -977.73 | -2.96 | 0.092 | 0.078 | 0.851 | [-29.2,-21.6] |
| $i$ | $i - z$ | 11.3 | 84.65 | 45.53 | 699.29 | 11.03 | 0.090 | 0.080 | 0.885 | [-26.1,-19.1] |

NOTE. — Parameters of the $LZC$ relation defined in Equation 1; $L$ is the photometric band of the luminosity, $\alpha$ is the optimal value of the color weighting factor to minimize the scatter in metallicity, and $p_l$ are the parameters of the best-fit $LZC$ polynomial for the corresponding value of $\alpha$. The value $\sigma_Z/\sigma_{Z,0}$ expresses the reduction in the scatter relative to the LZ relation (without color term). The range of $\mu$, the optimal projection of luminosity and color, over which the diagnostic is calibrated. The $\mu$ range is defined by the 2nd and 98th percentiles in $\mu$ (see Equation 1) of the SDSS galaxies in the calibration sample. Table 2 is published in its entirety in the electronic edition, including parameters for all metallicity diagnostics. A portion is shown here for guidance regarding its form and content.

for galaxies can be achieved with scatter $\delta z \sim 0.02$ (Ball et al. 2008), while $K$-corrections can be determined to $\lesssim 20\%$ (Blanton & Roweis 2007). In some applications of the $LZC$, galaxy redshift may already be known through e.g. observations of a hosted supernova. When using only 2 bands of photometry (the minimal use case for the $LZC$), $K$-corrections have a larger uncertainty (an additional scatter of $\sim 5 - 20\%$ versus full-photometric corrections; Chilingarian et al. 2010).

To test the uncertainty in metallicity introduced by use of photometric redshifts (photo-$z$) and 2-band $K$-corrections, we recompute metallicities for the subset of $\sim 70,000$ galaxies in the MPA-JHU catalog with photo-$z$ estimates in the SDSS-DR9. We use the $kd$-tree nearest neighbor fit photo-$z$ estimates, as described in Csabai et al. (2007). We compute $K$-corrections using the analytic prescriptions of Chilingarian et al. (2010), using both the spectroscopic and photometric redshifts for each galaxy. We apply the $LZC$ relation as calibrated for the

PP04 O3N2 metallicity diagnostic using the $M_g$ luminosities and $g - r$ colors (model magnitudes). The resulting distribution of metallicity residuals ($\delta Z$) for the spectroscopic versus photometric redshifts suggests that there is no systematic bias introduced by photo-$z$ (median $\delta Z = 0.000$ dex). The typical uncertainty added to the metallicity estimates is negligible (standard deviation $\delta Z = 0.008$ dex) and therefore the photometric metallicity estimate is dominated by the scatter in the $LZC$ relation.

Some additional properties of galaxies may effect their metallicity as estimated from the $LZC$ relation. Edge-on galaxies may be redder than face-on equivalents, leading towards an upward bias in their $LZC$ metallicity. Galaxy inclination could be included as an additional parameter in a future calibration of the $LZC$. Early-type galaxies may contaminate photometric samples of star-forming galaxies. Early-types should be excluded by careful application of color-magnitude diagrams; they may not lie
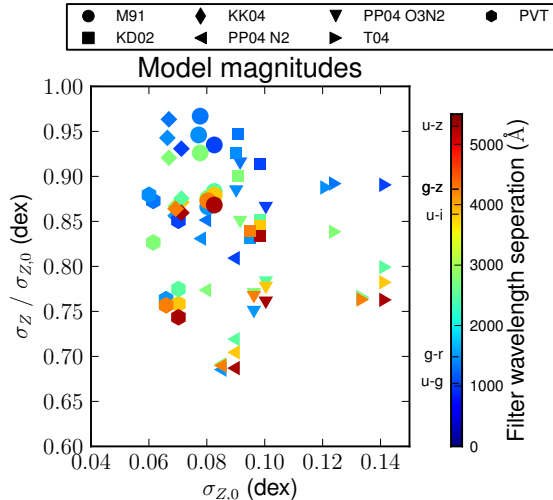
FIG. 3.— Summary statistics of the LZC calibrations. The axes show $\sigma_{Z,0}$, the scatter in metallicity around the luminosity-metallicity relation, and the ratio of $\sigma_Z$, the scatter in metallicity around the optimal LZC relation, to $\sigma_{Z,0}$. Smaller values on the $y$-axis represent improvement in scatter due to the addition of color information. Each point shown represents an independent calibration for a particular choice of luminosity filter, color filter pair (see color coding), and metallicity diagnostic (different symbols). The color coding is based on the seperation in Angstroms of the effective wavelength of the two color filters, and a few filter combinations are indicated in the colorbar at right. Only results from the model photometric method is shown – results for other methods are similar.

along the extrapolation of the LZC relation to redder colors, and the gas-phase metallicity of early-types may not be of interest in any case.

Fourth, we caution that the statistics presented here describe the bulk of the galaxy distribution (e.g. median and $1\sigma$ contours), while individuals may be outliers from this population. Like any photometric method for galaxy metallicity estimation, the LZC relations are most robust when applied to a statistical sample of galaxies.

## 5. APPLICATIONS

The calibrated LZC relation we present could benefit several disciplines, allowing for precise and accurate metallicity estimates for galaxies based on photometry alone. Spectroscopic metallicity measurement demands considerably more observational resources, while full SED modeling provides only weak constraints on metallicity ($1\sigma$ scatter of $\sim 0.2$ dex, e.g. Pacifici et al. 2012) and accesses the chemical composition in the older, stellar population rather than the gas phase. In contrast, the LZC relation can be employed to make precise measurements of gas phase metallicity using existing multi-band photometry from wide-field surveys such as SDSS or newly acquired, targeted observations, so long as an estimate for the redshift of each galaxy is available.

Studies of supernova (SN) host galaxies can support inferences into progenitor star populations (e.g. Modjaz et al. 2008; Prieto et al. 2008; Sanders et al. 2012b), with some studies relying on photometry rather than spectroscopy to measure the host galaxy metallicity (e.g. Prantzos & Boissier 2003; Boissier & Prantzos 2009; Arcavi et al. 2010). However, Sanders et al. (2012b) have shown that the statistical uncertainty associated with

metallicity estimates based on the galaxy luminosity-metallicity relation is a significant barrier to detecting subtle differences in metallicity among SN populations. Moreover, because some SNe strongly prefer blue galaxies (high SFR environments; Levesque et al. 2010; Kelly & Kirshner 2011), photometric metallicity estimates will be biased if color information is not incorporated. Using the LZC relation will effectively remove this bias, and significantly reduce the uncertainty in metallicity measurements. The additional uncertainty introduced by photo-$z$ should be minor, as SN host galaxies studies are almost exclusively done in the $z < 0.15$ regime (see compilation in Sanders et al. 2012b), and spectroscopic redshift estimates are often available from the SN spectroscopy. We note that the LZC relation predicts the galaxy metallicity in the inner few kpc of the galaxy, as probed by the $3''$ SDSS spectroscopic fibers, and significant offsets may exist from the SN host environment metallicity due to metallicity gradients in galaxies. However, these metallicity offsets are typically small ($\lesssim 0.1$ dex; Sanders et al. 2012b), and the intrinsic scatter in the radial metallicity profiles of galaxies limits observers' ability to spatially isolate the explosion site with spectroscopy (Rosolowsky & Simon 2008; Sanders et al. 2012a).

Similarly, galaxy metallicity measurements are key to the discussion of the progenitor properties of long-duration gamma-ray bursts (LGRBS, see e.g. Fynbo et al. 2003; Sanders et al. 2012c). While the host environments of LGRBs typically fall below the mass-metallicity relation (Levesque et al. 2010), it has been shown that these host galaxies do follow the fundamental plane relation (Mannucci et al. 2011, but see also Kocevski & West 2011). Because LGRBs are frequently discovered at high redshift ($z > 1$), the LZC relation could potentially be used to derive metallicity estimates at considerably lower expense than deep NIR spectroscopy (e.g. Maiolino et al. 2008). However, in order to study the high redshift extremely lowest metallicity environments preferred by LGRBs ($Z \lesssim 0.3 Z_\odot$, see e.g. Mannucci et al. 2011), additional calibration is needed to extend the LZC relation beyond the range probed by the SDSS galaxy sample, which is $0.4 Z_\odot \lesssim Z \lesssim 1.3 Z_\odot$ and $z < 0.3$ (with only 10% of the galaxies in our sample being at $0.2 < z < 0.3$).

As a usage example, we apply the LZC relation to the unusual host galaxy of the SN 2010ay. In Sanders et al. (2012c), we report that this host galaxy is a $2\sigma$ outlier from the luminosity-metallicity relation. The median and $1\sigma$ metallicity interval for SDSS galaxies with luminosity similar to this host galaxy ($M_B = -18.3$ mag) is $12 + \log(\text{O/H}) = 8.93 \pm 0.17$ (T04). This is a factor of $\gtrsim 2$ greater than the spectroscopically-measured T04 metallicity of $12 + \log(\text{O/H}) = 8.58$. The discrepancy is due to the extremely low mass-to-light ratio and high SFR of the host galaxy. The LZC relation cannot be applied in all filter combinations because the host lies outside the calibrated range for $\mu$. Using the LZC relation for $M_r$ and $r - i$ color, we find a T04 metallicity of $12 + \log(\text{O/H}) = 8.58 \pm 0.03$ (with an additional systematic uncertainty of 0.1 dex from the spread in the LZC relation). This agrees well with the spectroscopically measured value and has a significantly lower associated uncertainty than the estimate from the luminosity-

metallicity relation. Because the LZC relation cannot be applied in all filter combinations, this cases illustrates the importance of extending the calibration presented here to lower-metallicity host galaxies not well-represented in the SDSS spectroscopic sample.

Finally, we suggest that the next generation of wide field, multi-band, photometric surveys could use the *LZC* relation to characterize the metallicity distribution of galaxies in the local universe, and perhaps its evolution with redshift. The Pan-STARRS1 (PS1) survey is already operating, and will provide $g_{P1}$ $r_{P1}$ $i_{P1}$ $z_{P1}$ $y_{P1}$ photometry for $\sim 2 \times 10^8$ galaxies over 3/4 of the sky (Saglia et al. 2012). In the future, the Large Synoptic Survey Telescope (LSST) will provide *ugrizy* photometry of $\sim 10^{10}$ galaxies to $z \sim 6$ (LSST Science Collaboration et al. 2009). With the advent of such datasets, the *LZC* relation may play an important role in defining the metallicity distribution of galaxies that has emerged from the cosmic evolution of star formation and galaxy mass. To fulfill that role, the calibrations presented here must first be extended to higher redshift using data from ongoing spectroscopic surveys of the high redshift universe.

*Facilities:* PS1, EVLA, Swift, MMT

REFERENCES

Abazajian, K. N., et al. 2009, ApJS, 182, 543
Ahn, C. P., et al. 2012, ApJS, 203, 21
Andrews, B. H., & Martini, P. 2013, ApJ, 765, 140
Arcavi, I., et al. 2010, ApJ, 721, 777
Ball, N. M., Brunner, R. J., Myers, A. D., Strand, N. E., Alberts, S. L., & Tcheng, D. 2008, ApJ, 683, 12
Bell, E. F., & de Jong, R. S. 2001, ApJ, 550, 212
Blanton, M. R., & Roweis, S. 2007, AJ, 133, 734
Blanton, M. R., et al. 2005, AJ, 129, 2562
Boissier, S., & Prantzos, N. 2009, A&A, 503, 137
Brinchmann, J., Charlot, S., White, S. D. M., Tremonti, C., Kauffmann, G., Heckman, T., & Brinkmann, J. 2004, MNRAS, 351, 1151
Cardelli, J. A., Clayton, G. C., & Mathis, J. S. 1989, ApJ, 345, 245
Chilingarian, I. V., Melchior, A.-L., & Zolotukhin, I. Y. 2010, MNRAS, 405, 1409
Cresci, G., Mannucci, F., Sommariva, V., Maiolino, R., Marconi, A., & Brusa, M. 2012, MNRAS, 421, 262
Csabai, I., Dobos, L., Trencséni, M., Herczegh, G., Józsa, P., Purger, N., Budavári, T., & Szalay, A. S. 2007, Astronomische Nachrichten, 328, 852
Fynbo, J. P. U., et al. 2003, A&A, 406, L63
Garnett, D. R., & Shields, G. A. 1987, ApJ, 317, 82
Kauffmann, G., et al. 2003a, MNRAS, 346, 1055
——. 2003b, MNRAS, 341, 33
Kelly, P. L., & Kirshner, R. P. 2011, ArXiv e-prints, 1110.1377
Kewley, L. J., & Dopita, M. A. 2002, ApJS, 142, 35
Kewley, L. J., & Ellison, S. L. 2008, ApJ, 681, 1183
Kewley, L. J., Jansen, R. A., & Geller, M. J. 2005, PASP, 117, 227
Kobulnicky, H. A., Kennicutt, Jr., R. C., & Pizagno, J. L. 1999, ApJ, 514, 544
Kobulnicky, H. A., & Kewley, L. J. 2004, ApJ, 617, 240
Kocevski, D., & West, A. A. 2011, ApJ, 735, L8+
Lara-López, M. A., et al. 2010, A&A, 521, L53+
Lequeux, J., Peimbert, M., Rayo, J. F., Serrano, A., & Torres-Peimbert, S. 1979, A&A, 80, 155
Levesque, E. M., Kewley, L. J., Berger, E., & Zahid, H. J. 2010, AJ, 140, 1557

Lopez-Sanchez, A. R., Dopita, M. A., Kewley, L. J., Zahid, H. J., Nicholls, D. C., & Scharwachter, J. 2012, ArXiv e-prints, 1203.5021
LSST Science Collaboration, et al. 2009, ArXiv e-prints, 0912.0201
Maiolino, R., et al. 2008, A&A, 488, 463
Mannucci, F., Cresci, G., Maiolino, R., Marconi, A., & Gnerucci, A. 2010, MNRAS, 408, 2115
Mannucci, F., Salvaterra, R., & Campisi, M. A. 2011, MNRAS, 439
McGaugh, S. S. 1991, ApJ, 380, 140
Modjaz, M., et al. 2008, AJ, 135, 1136
Osterbrock, D. E., & Ferland, G. J. 2006, Astrophysics of gaseous nebulae and active galactic nuclei, ed. Osterbrock, D. E. & Ferland, G. J.
Pacifici, C., Charlot, S., Blaizot, J., & Brinchmann, J. 2012, MNRAS, 421, 2002
Padmanabhan, N., et al. 2008, ApJ, 674, 1217
Peeples, M. S., & Shankar, F. 2011, MNRAS, 417, 2962
Perez-Montero, E., et al. 2012, ArXiv e-prints, 1210.0334
Pettini, M., & Pagel, B. E. J. 2004, MNRAS, 348, L59
Pilyugin, L. S., Vílchez, J. M., & Thuan, T. X. 2010, ApJ, 720, 1738
Prantzos, N., & Boissier, S. 2003, A&A, 406, 259
Prieto, J. L., Stanek, K. Z., & Beacom, J. F. 2008, ApJ, 673, 999
Rosolowsky, E., & Simon, J. D. 2008, ApJ, 675, 1213
Saglia, R. P., et al. 2012, ApJ, 746, 128
Salim, S., et al. 2007, ApJS, 173, 267
Sanders, N. E., Caldwell, N., McDowell, J., & Harding, P. 2012a, ApJ, 758, 133
Sanders, N. E., et al. 2012b, ApJ, 758, 132
——. 2012c, ApJ, 756, 184
Schlegel, D. J., Finkbeiner, D. P., & Davis, M. 1998, ApJ, 500, 525
Stoughton, C., et al. 2002, AJ, 123, 485
Tremonti, C. A., et al. 2004, ApJ, 613, 898
Yates, R. M., Kauffmann, G., & Guo, Q. 2012, MNRAS, 422, 215